SEMARAK ILMU PUBLISHING

Journal of Advanced Research in Fluid Mechanics and Thermal Sciences

Journal homepage:
https://semarakilmu.com.my/journals/index.php/fluid_mechanics_thermal_sciences/index
ISSN: 2289-7879

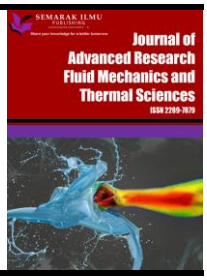

A Computational Technique for Low-Cycle Fatigue of LNG Mixing-Tee Weldment – An Industry Case Study

Abdul Matin Al-Barr Malek[1,2], Abdul Rahim Othman[1,*], Muhammad Firdaus Othman[2]

[1] Mechanical Department, Universiti Teknologi PETRONAS, Seri Iskandar, Malaysia
[2] Group Technical Solution, Level 15, Tower 3, KLCC, Kuala Lumpur, Malaysia

ARTICLE INFO

Article history:
Received 20 December 2022
Received in revised form 5 March 2023
Accepted 13 March 2023
Available online 27 March 2023

Keywords:
Computational analysis; mixing-tee; liquefied natural gas; fatigue life cycle; thermal stress

ABSTRACT

This research describes a computational method for low-cycle fatigue cracks in LNG mixing-tee weldments. Using a combination of thorough finite element modelling and fatigue life prediction with the finite element software ABAQUS and FE-Safe, the approach is able to simulate the thermal stresses and fatigue damage of a mixing-tee subjected to thermal cycle. The approach consists of three primary phases. First, the thermal distribution at the mixing-tee junction caused by the mixing temperature of the liquefied natural gas (LNG) is predicted. These first-step solutions are then included into second-step modelling, which simulates the thermal stress of the mixing-tee. The next phase entails modelling the fatigue behaviour of the mixing-tee using the thermal stress data. The computed fatigue life cycle achieves a 92.8% accuracy level when compared to real on-site observations. The suggested method enables the accurate prediction of thermal and fatigue behaviours within a tolerable computational time.

1. Introduction

At an LNG facility, the mixing-tee is commonly utilised in the dehydration unit's gas reactivation system, where it runs in thermal-cyclical mode. The full cycle of the reactivation procedure begins with a cold working temperature, increases to a hot temperature, and finally returns to the initial temperature. Depending on the operating process, thermal-cyclic operation occurs many times each day at the mixing-tee. In addition, the mixing-tee undergoes thermal stripping, resulting in the mixing of hot and cold fluids at its connections [1]. The temperature gradient at the mixing joint offers useful information on the mechanical response of the tee, i.e., thermal stress. In their flow pattern investigation, Ogawa *et al.,* [2] and Hosseini *et al.,* [3] revealed the temperature distribution of mixing-tee. Their analysis detailed the flow pattern and temperature distribution of the fluids [4] from the mixing tee to the pipe itself. Instead, the heat distribution can be confirmed by measuring the skin temperature on-site.

* *Corresponding author.*
E-mail address: rahim.othman@utp.edu.my

https://doi.org/10.37934/arfmts.104.2.103114

The National Association of Corrosion Engineers has offered a solution for mixing-tee problems in NACE SP0114 for designing process mix points, including quills, spray nozzles, thermal sleeves, and static mixer [5]. In JSME S017, the Japan Society of Mechanical Engineers also produced a design guideline for mixing-tees. The guideline gives a method for identifying the flow pattern, performing numerical analysis, and anticipating the initiation of fatigue damage [6]. Using a spray nozzle, Gao *et al.,* [7] discovered in 2015 that the temperature fluctuation in mixing-tee was decreased precisely at the inner wall surface. The research indicated that incorporating a spray nozzle into a mixing-tee considerably enhanced the efficiency of the mixing operation [7,8]. Alec Pattinson *et al.,* [9] conducted other study in 2014 to measure the importance of thermal sleeves on mixing-tees subjected to fluctuating temperature and pressure conditions.

Most comparable research on numerical analysis were undertaken by Courtin [10] for high-cycle thermal fatigue of mixing-tee at a nuclear power plant to examine variable of fatigue loading, cycle counting technique, and selection of fatigue design curve to fracture initiation time. S. Courtin suggested that the cycle counting method selection significantly impacts the crack initiation time compared to fatigue loading or the fatigue material criterion. Recent research by Kim *et al.,* [11] investigates the effect of seismic loading on nuclear plant pipe systems susceptible to low-cycle fatigue degradation. In addition, Varelis and Karamanos [12] and Jang *et al.,* [13] utilised a numerical model for a pipe elbow exposed to low-cycle fatigue in their research. Their improvised solution incorporated a tie-break strategy, which enhanced computational time without compromising experimental results.

Many recognised fatigue damage criteria and mean stress effects models may be utilised to estimate the remaining life for low-cycle fatigue [14] as tabulated in Table 1 and Table 2, respectively. API 579-1 advocated the use of the Brown-Miller criterion model for fatigue evaluation. Brown-Miller proposed that the fatigue crack occurs on the maximum shear strain amplitude plane, and the strain is normal to this plane [15]. The Brown-Miller approach provides the most accurate life calculation for ductile metals [16]. For high cycle fatigue difficulties, mean stress correction models play a crucial role in determining material fatigue strength.

Low cycle fatigue, on the other hand, is linked with substantial plastic deformation rather than the mean stress effect. Bader and Kadum [17] conducted experiments on the mean stress correction effects of steel alloys and concluded that Soderberg and Goodman are the best models for steel alloys with a higher carbon content. Lee *et al.,* [18] done more work on the fatigue damage model to express the hardening effect by altering the von Mises equivalent stress amplitude. In addition, Bomas *et al.,* [19] conducted an experiment on normalised low-carbon steel thin-walled tubulars exposed to cyclic loads in many planes.

Table 1
Low cycle fatigue criteria models

Model	Relationship
Morrow	$\frac{\Delta\varepsilon}{2} = \frac{\sigma_f' - \sigma_m}{E}(2N_f)^b + \varepsilon_f'(2N_f)^c$
Smith-Watson-Topper	$\frac{\Delta\varepsilon}{2}\sigma_{max} = \frac{\sigma_f'^2}{E}(2N_f)^{2b} + \varepsilon_f'\sigma_f'(2N_f)^{b+c}$
Manson	$\varepsilon = 3.5\,\frac{\sigma_{uts}}{E}N_f{}^{-0.12} + \varepsilon_f^{0.6}N_f{}^{-0.6}$
Brown-Miller	$\left(\frac{\Delta\gamma}{2} + \frac{\Delta\varepsilon_n}{2}\right)_{max} = 1.65\frac{\sigma_f' - \sigma_m}{E}(2N_f)^b + 1.75\varepsilon_f'(2N_f)^c$

Table 2
Mean stress correction models for stress-life approach

Model	Relationship	Features
Gerber	$\frac{\sigma_a}{\sigma_{ar}} + \left(\frac{\sigma_m}{\sigma_u}\right)^2 = 1$	Suitable for ductile material
Goodman	$\frac{\sigma_a}{\sigma_{ar}} + \frac{\sigma_m}{\sigma_u} = 1$	Suitable for brittle material
Soderberg	$\frac{\sigma_a}{\sigma_{ar}} + \frac{\sigma_m}{\sigma_y} = 1$	Most conservative
Morrow	$\frac{\sigma_a}{\sigma_{ar}} + \frac{\sigma_m}{\sigma'_f} = 1$	Based on fatigue strength coefficient

International standards have set the solutions and design methodology for mixing-tees. Nevertheless, there is no specific finite element analysis guideline for determining the fatigue life of mixing-tee weldments that have been installed on-site for several years.

The current work presents and discusses an industrial case study of LNG mixing-tee weldment [20] subjected to low-cycle fatigue quantification. This work proposes analysing low cycle fatigue computational technique on mixing-tee weldment in an LNG processing plant. The numerical results from this work will be directly compared to the actual industrial case study of LNG mixing-tee.

1.1 Mixing-Tee Piping System

This study centred on the mixing-tee commonly employed in the gas reactivation system of a dehydration plant running in a thermal-cyclic mode. The actual shape and dimensions of the mixing-tee are utilised for modelling and evaluation. The detail of the mixing-tee was extracted from piping isometric, site measurement and related documents. The overview and geometry details of the mixing tee are tabulated in Table 3.

The mixing-tee is subjected to cyclic thermal operating four times daily during the operating condition. The first crack was observed at the outlet mixing-tee weldment after seven years in operation. The weldment was repaired and put back into service. The cyclic process parameter was changed from four times to three times daily. However, the fire incident reoccurred after ten years in service on the same outlet mixing-tee weldment. The failure of mixing-tee weldment resulted in a loss of pressure containment of hydrocarbon, causing fire and plant shutdown. A root cause failure analysis suggested that the failure of mixing-tee weldment was caused by fatigue damage from the thermal cyclic operating process.

Table 3
Overview of mixing-tee piping system

Description	Mixing-tee	Pipe
Construction code	ASME B16.9	ASME B36.10
Size	12"- SCH 60	12"- SCH 60
Construction materials	Stainless steel, A 403 WP304H	Stainless steel, A 312 WP304H
Outer Diameter (mm)	324	324
Internal Diameter (mm)	282	295
Thickness (mm)	21	14
Operating pressure (MPa)	6.65	
Inlet hot design temperature (°C)	360	
Inlet cold design temperature (°C)	21	
Outlet design temperature (°C)	320	

Low-cycle thermal fatigue phenomena may occur when the system operates in cyclic thermal conditions. The accumulated strains resulting from cyclic thermal loading on the mixing-tee weldment surface could initiate the fatigue crack [21].

2. Methodology

2.1 Finite Element Analysis

Finite element software Abaqus v6.14-3 was used to perform the modelling analysis. The piping system consists of modelled pipe and tee components, as illustrated in Figure 1 [22]. The model was constructed using solid element type. The weldment sections were constructed based on "thicker pipe taper-bored to align", as specified in ASME B31.3 [23].

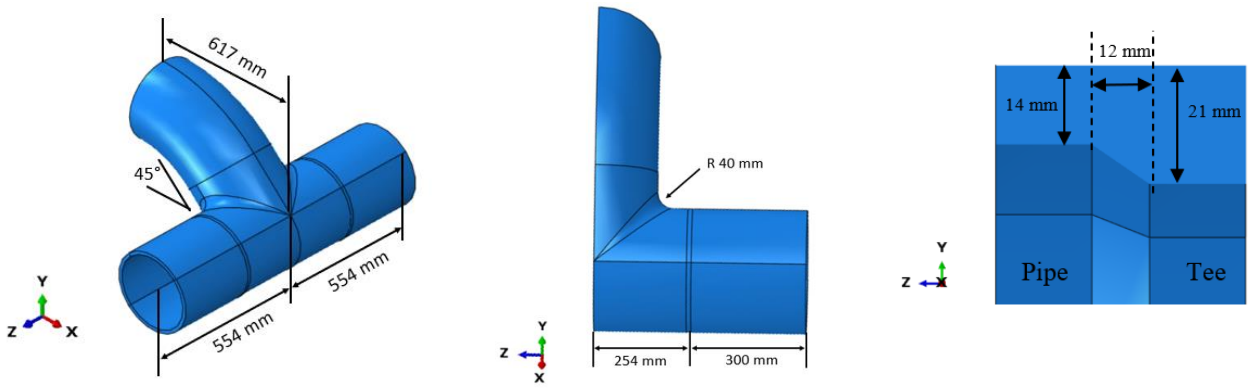

Fig. 1. Illustration of overall mixing-tee model

Kinematic coupling boundary conditions were employed with all degree-of-freedom fixed, except in radial direction. These boundary conditions were specified to allow for model expansion in the radial direction due to internal pressure. The material A312 WP304H was used for the analysis, and the properties are defined according to ASME Section II Part D [24]. The mean thermal expansion coefficient (Coefficient B) was chosen for the thermal expansion. The reference temperature was set at 20°C, consistent with the ASME database. The material properties of A312 WP304H used in the analysis are summarized in Table 4.

Table 4
The material properties for the A312 WP304H [24]

Description	Parameter
Material model	Elastic
Young's modulus (GPa)	195 – 174 @ 20 °C to 300 °C (Lower-bound values)
Poisson's ratio	0.3
Density (kg/mm^3)	7980
Thermal expansion coefficient (10^{-6} mm/mm/°C)	16.4 – 17.7 @ 20 °C to 320° C
Thermal conductivity (W/m°C)	14.8 -19.8 @ 20 °C to 320° C
Specific heat, c_p (J/kg °C)	477 - 557 @ 20 °C to 320° C

The model was meshed using a combination of quadratic order elements of tetrahedron elements (C3D10) and hexahedral elements of reduced integration solid element (C3D20R), as shown in Figure 2. A minimum of three elements in the through-thickness direction was used based on the sensitivity analysis conducted. Mesh sizing was set at three elements by number method and global mesh seed size, with the overall mixing-tee model set at seven with a curvature control option.

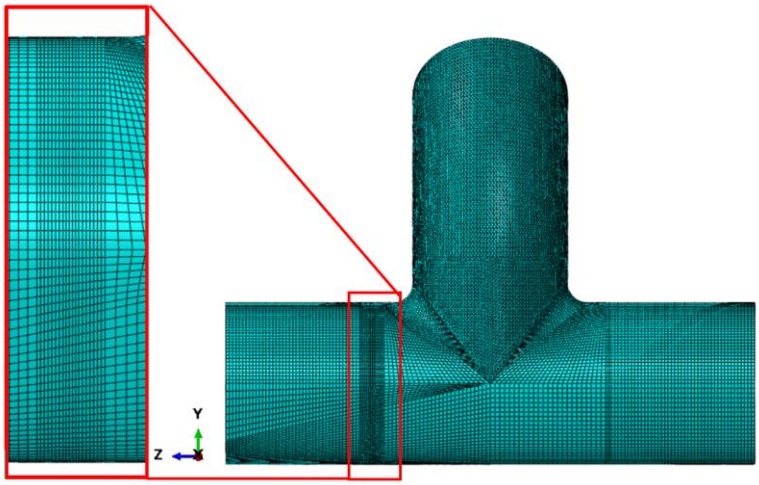

Fig. 2. Overall mesh arrangement for the mixing-tee, higher density mesh was used at the mixed-weldment (area of interest)

2.2 Thermal Analysis of Mixing-Tee

An initial thermal analysis was conducted before the thermal stress analysis to determine the temperature profile at the mixing tee. The surface film condition method of a coefficient of 0.6 was used in this analysis with the transient technique. The initial surface temperature was applied at three central regions; (a) Cold, (b) Hot, and (c) Mixed, as shown in Figure 3.

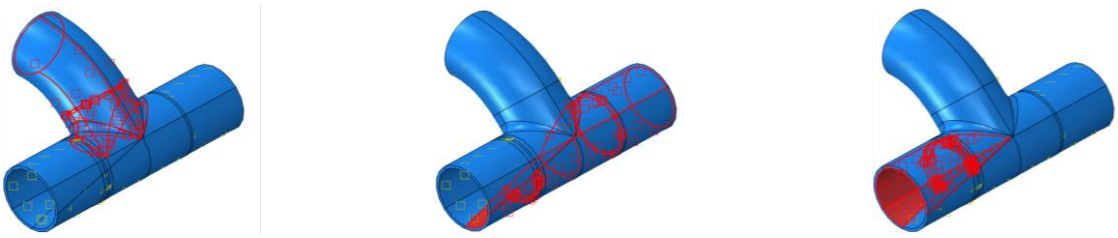

(a) (b) (c)

Fig. 3. Three regions assigned for temperature (a) Cold (b) Hot (c) Mixed

To simulate the actual operational condition of the mixing-tee, the actual temperature parameter and data trending from plant data history were used for the cyclic thermal loading. The temperature cycle data was plotted based on the Rainbow Cycle Counting method as recommended by API [14]. The three seconds were used with an increment size of the 0.5-time step to attain 6-time steps in one thermal cycle. Temperature for the cold section was maintained at 21°C throughout the time step. For the other two sections, the temperatures were assigned based on Rainflow Cycle Counting [16] temperature cycle for each time step as shown in Figure 4 for each time step.

2.3 Thermal Stress Analysis of Mixing-Tee

Subsequently, the thermal stress analysis model was developed for one cycle with incremental time steps of three and an increment of 0.5. The temperature distribution of each time step from the thermal analysis was used as inputs for thermal loading. In addition, the internal pressure was applied at a design value of 6.65 MPa, consistently throughout the analysis, regardless of the time step.

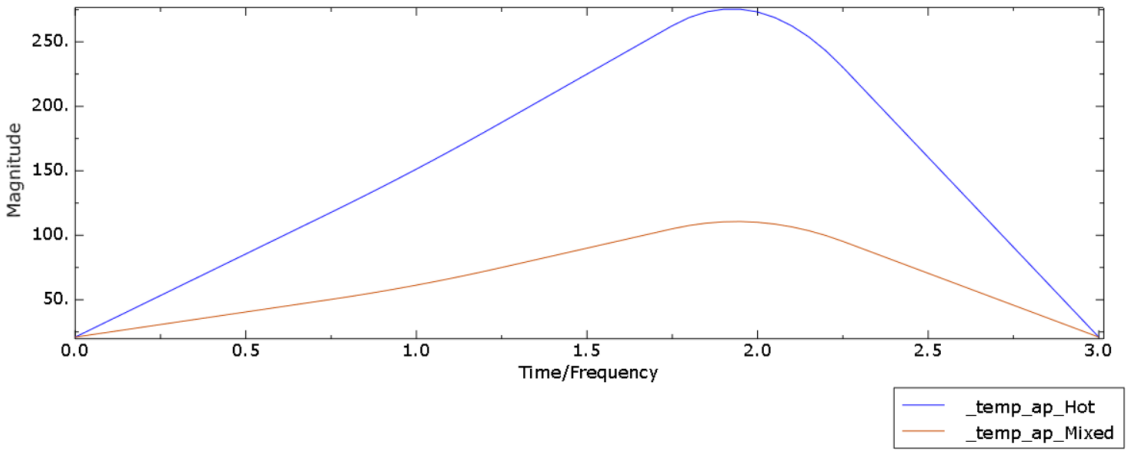

Fig. 4. The temperature plot at every time step for hot and mixed region in one cycle

The actual loading conditions imposed in the mixing-tee system were rather complex. A global model of the overall piping system was developed before this work to determine the pipe displacement connected to mixing-tee piping. The global model was developed using Caesar II software v2019, consisting of simplified three pressure vessels, piping, and valves. The displacement values in the x, y, and z axes and rotation Rx, Ry and Rz at the end of each mixing tee are extracted accordingly. These values were then calculated to find relative displacement and rotation as inputs to the coupling mixed-pipe end section, as tabulated in Table 5. On the other hand, the boundary conditions at the other two couplings were fixed in all degrees of freedom (DOF).

Table 5
Displacement and rotation data set for coupling-Mixed-Pipe according to each time step

Displacement/ rotation	Time Step			
	0	1	2	3
x (mm)	-0.061	-0.814	-5.000	-0.061
y (mm)	-1.002	-1.898	-2.409	-1.002
z (mm)	0.853	5.947	15.173	0.853
Rx (rad)	0.000108	0.000314	0.000412	0.000108
Ry (rad)	0.000010	-0.000099	-0.000600	0.000010
Rz (rad)	0.000056	-0.000033	-0.000220	0.000056

2.4 Fatigue Analysis

Fatigue analysis was conducted using FE-Safe 2019 software [23,24], with the output of thermal stress analysis used as an input for the analysis. The analysis focused on the area of interest in the Mixed-Weldment section rather than the whole model. This step is vital to reduce the computational time of fatigue analysis [25], as the interested section only consisted of 7,866 surface elements, compared to 166,802 surface elements for the whole model.

The fatigue response of one cycle of thermal stress was determined. Therefore, the stress datasets of 1, 2 and 3 were set to increase from 0 to 1 in the time history. The fatigue material model of SAE-30304 was selected as the material input, with the material fatigue properties tabulated in Table 6.

The Brown-Miller algorithm with Morrow means stress correction was used in the analysis as per API [14]. In addition, the surface finish factor, Kt, for each element and node group was also set as 1, representing the default material as a smooth surface. Results of the analysis will be given in log-life scale, where the actual fatigue cycle can be determined using Eq. (1). The fatigue cycles were then divided by the number of cycles per year to obtain the predicted fatigue life.

$$\text{Fatigue cycle} = 10^{\log-\text{life}} \tag{1}$$

Table 6
Material fatigue properties of SAE-30304 material

Description	Parameter
Constant amplitude endurance limit, 2nf	2E7
Young's Modulus, E (MPa)	186165
Poisson's ratio	0.33
Ultimate Tensile Strength, UTS (MPa)	572
Cyclic strain hardening coefficient, K' (MPa)	2275
Cyclic strain hardening exponent, n'	0.334
Fatigue strength exponent, b	-0.139
Fatigue strength coefficient, sf' (MPa)	1267 MPa
Fatigue ductility exponent, c	-0.415
Sn curve: N value, nf	10000, 1E6
Sn curve: S value (MPa)	537.8, 273.3

3. Results

3.1 Thermal Transient Analysis

The thermal profile obtained from the thermal analysis indicates the mixing thermal profile at the junction of the mixing-tee due to the mixing of the hot and cold medium. The thermal analysis results were validated with the measured skin temperature of the mixing-tee system at the LNG plant. Initially, the thermal profile at time step 2 during the end of the 'Heating Ramp' stage was compared to the site temperature measurement, as shown in Figure 5(a) and (b). The comparison suggested that the temperature profile matched the site temperature condition closely. The temperature results were extracted and plotted in Figure 5(c), with line extraction as shown in Figure 5(b). Correlation, root mean squared error (RMSE), and coefficient of determination between thermal analysis data series and site temperature measurement data series were calculated at 0.969, 0.064 and 0.958, respectively. The results indicated good arrangement between the model and measured data, ensuring that the thermal effect on the stress analysis was reflecting the site condition correctly, to some extent.

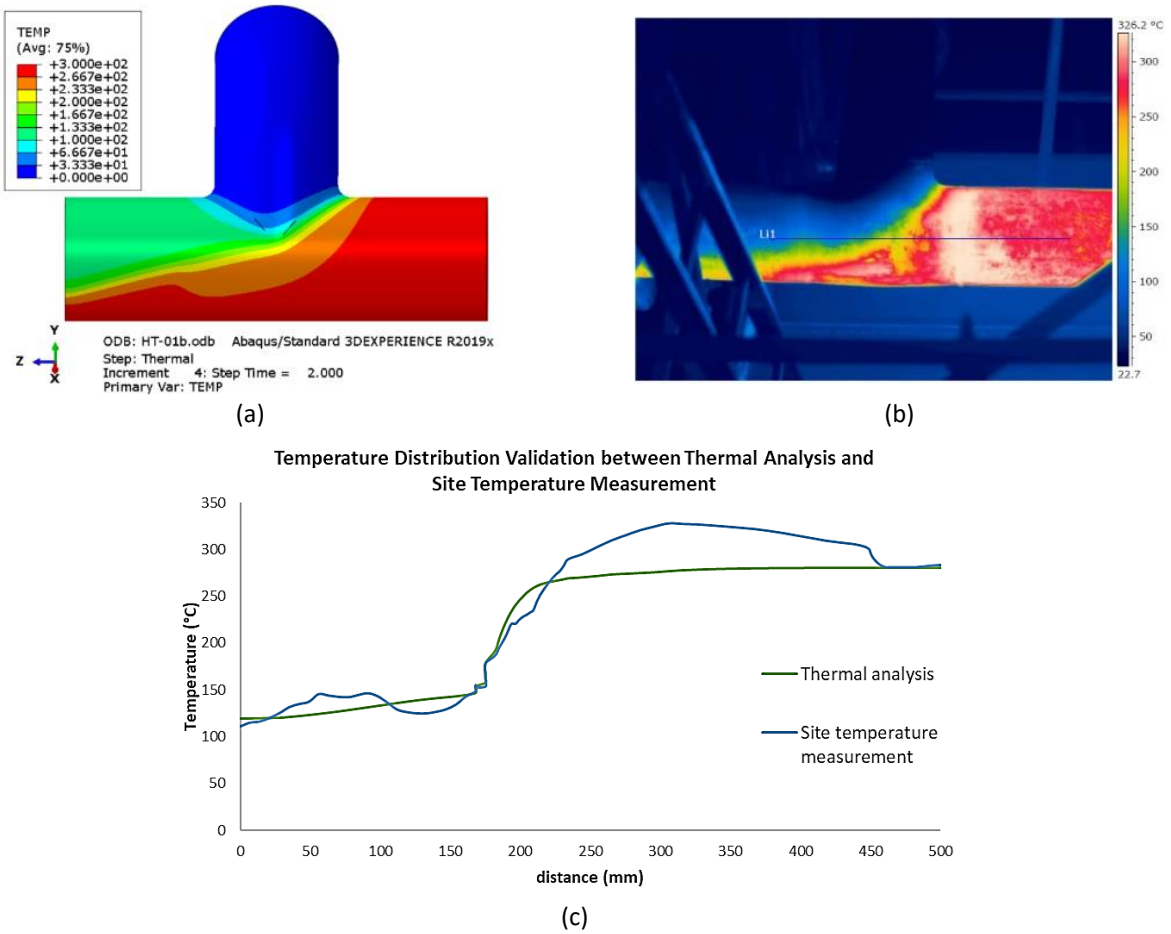

Fig. 5. Comparison of the temperature distributions (a) Thermal analysis at time step 2 (b) Skin temperature measured at site (c) Temperature distributions plot of the thermal analysis results for site

3.2 Thermal Stress Analysis

Stress results were presented at the end of one thermal cycle. Stresses and elastic strains were extracted at two conditions; (i) end of the 'Heating Ramp' when the inlet section reached the maximum temperature of 300°C, at time step 2, and (ii) end of the 'Purging' stage when the inlet section reduced to 21°C, at time step 3. This is important to determine the total accumulated stresses and elastic strains due to the thermal cycle at the end of the cycle. The radial, tangential, and axial components at the area of interest of Mixed-Weldment were extracted in detail using a cylindrical coordinate axis. The maximum stresses and elastic strain obtained from the thermal stress analysis are summarized in Table 7.

Table 7
Summary of thermal stress analysis

Component	Time step 2 Max. Stress (MPa)	Location	Time step 3 Max. Stress (MPa)	Location
von Mises	634	3 o'clock at inner diameter	194	11 o'clock at inner diameter
Radial	55	8 o'clock at inner diameter	27	11 o'clock at inner diameter
Tangential	237	1 o'clock at inner diameter	132	5 o'clock at inner diameter
Axial	432	8 o'clock at inner diameter	218	11 o'clock at inner diameter
Component	Max. Elastic Strain (%)	Location	Max. Elastic Strain (%)	Location
Max Principal	0.217	8 o'clock at inner diameter	0.102	11 o'clock at inner diameter
Radial	0.107	4 o'clock at inner diameter	0.007	6 o'clock at outer diameter
Tangential	0.157	4 o'clock at outer diameter	0.007	6 o'clock at outer diameter
Axial	0.198	8 o'clock at inner diameter	0.094	11 o'clock at inner diameter

Figure 6 presents the results of fatigue simulation at the Mixed-Weldment of the mixing-tee model, indicating a log-life value of 4.007, equivalent to 104.007 fatigue life cycle. The calculated number of the fatigue life cycle for the mixing model was deduced at 10220 cycles. The results of the fatigue simulation were validated with the inspection report from the site, measured during a crack monitoring event in 2017. The inspection was performed using the ultrasonic test method. The location and characteristics of the crack damage were compared between the fatigue simulation results and the inspection report. The comparison results were established and summarized in Table 8.

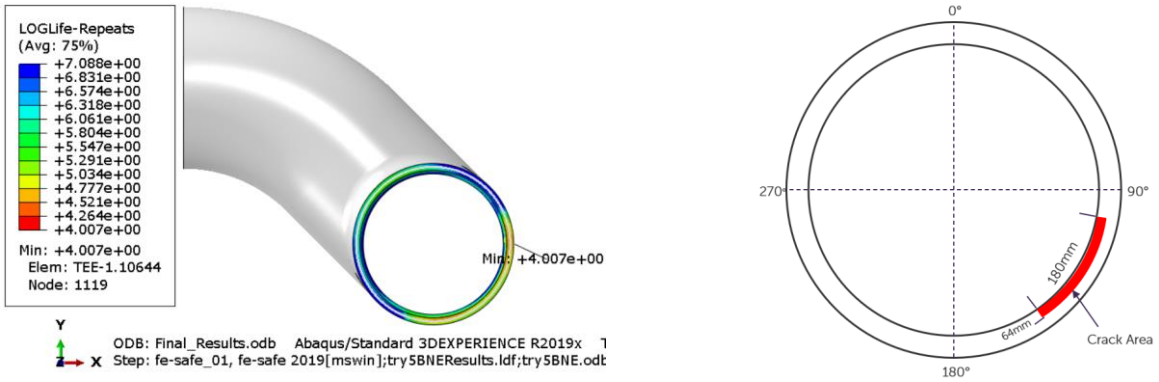

(a) (b)

Fig. 6. (a) High damage area concentration located at inner weldment of 3 to 6 o'clock orientation (b) Location of the crack based on the inspection report and validated with the simulation results

The damage simulated from the fatigue simulation analysis reflected similar characteristics of the crack reported at the site. However, no record of the crack initiation location was reported at the mixing tee. Nevertheless, the high damage concentration at the Mixed-Weldment location observed from the FE analysis matched the inspection. The fatigue analysis has identified the area of damage from 3 to 6 o'clock of the inner weldment area, as shown in Figure 6. Whereas it was reported that the location of the crack was at approximately 3 to 5 o'clock orientation, observed during the inspection event.

Table 8
Summary of fatigue simulation results against inspection report findings

Characteristic	Fatigue simulation result	Inspection report finding
Location of the damage	Damage was found located at the weldment area	Crack was found located at the weldment area
Location across thickness	Damage was found and initiated from inner diameter of the weldment area	Crack was found propagated from inner to outer diameter of the weldment
Damage/Crack area	Most extreme damage located at 3 o'clock orientation. High damage concentration was found from 3 to 6 o'clock orientation.	Crack was identified located at approximately 3 to 5 o'clock orientation with 180 mm length and 8.48 mm depth.

Further assessment was performed to verify a number of cycles based on two incidents of fatigue damage. The first fatigue damage occurred at the LNG plant in 2007, with an operating period of 7 years, as the equipment operated at four cycles per day. The crack at the mixing-tee was repaired and put back into service, with the operation procedure changed to 3 cycles per day. The following incident recurred in 2017 with an operating period of 10 years. Based on the information, the number of cycles for these two incidents was calculated based on the fatigue simulation result. The incident in 2007 contributed 6.961 years of fatigue life, whereas the incident in 2017 was calculated at 9.281 years, with a percentage error of 0.6% and 7.2% from actual incidents, respectively. The details of fatigue assessment results are tabulated in Table 9.

Table 9
Comparison of simulation and actual fatigue damage at site

Description	First incident (2000-2007)		Second incident (2007-2017)	
	Actual	Simulation	Actual	Simulation
Fatigue life in log-life	N/A	4.007	N/A	4.007
Number of cycle (cycle)	10220	10162	10950	10162
Operational cyclic (cycle/day)	4	4	3	3
Accumulated damage (year)	7.000	6.961	10.000	9.281

4. Conclusions

A computational technique for analysing low cycle fatigue on mixing-tee weldment is presented. The finite element formulation within ABAQUS software was used to quantify the mixing-tee's thermal profile and the resultant stresses. The cyclic life of the mixing-tee due to the thermal cyclic process was quantified using the critical plane approach in FE-Safe. The proposed technique provides a high level of accuracy in determining the thermal stress and fatigue cycle life of mixing-tee subject to thermal cyclic and complex temperature distributions. Based on the grounds of results accuracy, the FE model provides high-level accuracy with a maximum percentage difference of 1.22% compared with the actual finding at the site. The results presented in this paper support the following conclusion

i. The thermal profile obtained from the thermal analysis indicates the mixing thermal profile at the junction of the mixing-tee due to the mixing of the hot and cold medium. The mixing thermal profile from the FE model matched the finding at the site.
ii. The thermal stress profile after the Heating ramp and purging stage indicates the maximum stress value at the inner diameter of discontinuity between weldment and piping.

iii. The damage simulated from the fatigue simulation analysis reflected similar characteristics of the crack reported at the site. The fatigue analysis findings indicated serious damage area of the inner weldment area at 3 to 6 o'clock, which agreed well with the crack location reported during the inspection.

iv. The calculated fatigue life cycle of the mixing-tee based on the proposed technique provides an accuracy of at least 92.8 % as compared to the actual cycle life deduced from the actual incidents.

Acknowledgement
The authors gratefully acknowledge the UTP National Collaborative Research Fund (NCRF) for funding support (cost centre: 015MD0-121), as well as Digital Analytics Structural Integrity Technology (DASIT), Universiti Teknologi PETRONAS, for technical support.

References

[1] Kawasaki, N., N. Kasahara, and H. Takasho. "Thermal fatigue evaluation of partially cooled pipes." (2004).
[2] H. Ogawa, M. Igarashi, N. Kimura and H. Kamide. "Experimental Study on Fluid Mixing Phenomena in T-pipe Junction with Upstream Elbow." *The 11th International Topical Meeting on Nuclear Reactor Thermal-Hydraulics,* (2005): 448. https://doi.org/10.1016/j.nucengdes.2010.05.019
[3] Hosseini, Seyed Mohammad, Kazuhisa Yuki, and Hidetoshi Hashizume. "Classification of turbulent jets in a T-junction area with a 90-deg bend upstream." *International Journal of Heat and Mass Transfer* 51, no. 9-10 (2008): 2444-2454. https://doi.org/10.1016/j.ijheatmasstransfer.2007.08.024
[4] Misaran, Mohd Suffian, Cheng Fang Sing, and Mohd Adzrie. "Study of wyee-tee duck design at various protrusion and guide vane location using CFD." *CFD Letters* 11, no. 11 (2019): 39-47.
[5] Injection, Refinery. "Standard Practice Refinery Injection and Process Mix Points." (2014).
[6] Kamaya, Masayuki, Yoichi Utanohara, and Akira Nakamura. "Thermal fatigue analysis at a mixing tee by a fluid-structural simulation." In *Pressure Vessels and Piping Conference*, vol. 44519, pp. 383-391. 2011. https://doi.org/10.1115/PVP2011-57585
[7] Gao, Kai, P. Wang, Tao Lu, and Terry Song. "Experimental investigation and numerical simulation for weakening the thermal fluctuations in a T-junction." *Annals of Nuclear Energy* 78 (2015): 180-187. https://doi.org/10.1016/j.anucene.2015.01.001
[8] Suzuki, Shigeki, Koichi Tanimoto, and Yoshiyuki Kondoh. "Prevention of piping high cycle thermal fatigue at design stage." (2005).
[9] Pattinson, Alec, James Dodds, Peter Hugill, and Gary Reed. "Finite Element Analysis of a Pipe Junction with a Thermal Sleeve Subject to Thermal and Pressure Transient Events." In *Pressure Vessels and Piping Conference*, vol. 46001, p. V003T03A022. American Society of Mechanical Engineers, 2014. https://doi.org/10.1115/PVP2014-28125
[10] Courtin, Stéphan. "High cycle thermal fatigue damage prediction in mixing zones of nuclear power plants: engineering issues illustrated on the FATHER case." *Procedia Engineering* 66 (2013): 240-249. https://doi.org/10.1016/j.proeng.2013.12.079
[11] Kim, Sung-Wan, Bub-Gyu Jeon, Dae-Gi Hahm, and Min-Kyu Kim. "Seismic performance limit of nuclear power plant piping system with seismic isolation system considering measurement points: Damage index." *Engineering Failure Analysis* 130 (2021): 105742. https://doi.org/10.1016/j.engfailanal.2021.105742
[12] Varelis, George E., and Spyros A. Karamanos. "Low-cycle fatigue of pressurized steel elbows under in-plane bending." *Journal of Pressure Vessel Technology* 137, no. 1 (2015). https://doi.org/10.1115/1.4027316
[13] Jang, Heung Woon, Daegi Hahm, Jae-Wook Jung, and Jung-Wuk Hong. "Effective numerical approach to assess low-cycle fatigue behavior of pipe elbows." *Nuclear Engineering and Technology* 50, no. 5 (2018): 758-766. https://doi.org/10.1016/j.net.2018.01.020
[14] American Petroleum Institute (Wash.). *Fitness-for-service: API 579-1/ASME FFS-1, June 5, 2007*. American Petroleum Institute, 2007.
[15] Bathias, Claude, and André Pineau, eds. *Fatigue of materials and structures: application to design and damage*. John Wiley & Sons, 2013. https://doi.org/10.1002/9781118616994
[16] Fatigue Theory Reference Manual. (2002). *Intergraph*, vol. 2. Safe Technilogy Limited.
[17] Bader, Qasim, and Emad Kadum. "Mean stress correction effects on the fatigue life behavior of steel alloys by using stress life approach theories." *Int. J. Eng. Technol* 14, no. 04 (2014): 50-58.

[18] Lee, Yung-Li, Tana Tjhung, and Algernon Jordan. "A life prediction model for welded joints under multiaxial variable amplitude loading histories." *International Journal of Fatigue* 29, no. 6 (2007): 1162-1173. https://doi.org/10.1016/j.ijfatigue.2006.09.014
[19] Bomas, H., M. Lohrmann, G. Löwisch, and P. Mayr. "Multiaxial low cycle fatigue of a normalized carbon steel." *Low Cycle Fatigue and Elasto-Plastic Behaviour of Materials—3* (1992): 362-368. https://doi.org/10.1007/978-94-011-2860-5_59
[20] Khattak, M. A., K. Azam Khan, and A. Mukhtar. "Common root causes of pressure vessel failures: a review." *Journal of Advanced Research in Applied Mechanics* 21, no. 1 (2016): 22-37.
[21] Ellingwood, B. R. "Probabilistic assessment of low-cycle fatigue behavior of structural welds." (1976): 26-32. https://doi.org/10.1115/1.3454319
[22] Halim, Nur Fazlin Che, and Nor Azwadi Che Sidik. "Mixing Chamber for Preparation of Nanorefrigerant." *Journal of Advanced Research in Applied Sciences and Engineering Technology* 21, no. 1 (2020): 32-40. https://doi.org/10.37934/araset.21.1.3240
[23] The American Society of Mechanical Engineers. (2018). Process Piping, ASME B31.3 vol. 2018.
[24] The American Society of Mechanical Engineers. (2013). Material (Metric). ASME BPVC Section II Part D. ASME.
[25] Venugopal, Arvinthan, Roslina Mohammad, and Md Fuad Shah Koslan. "Fatigue Crack Growth Prediction on Su-30MKM Horizontal Stabilizer Lug Using Static Analysis." *Journal of Advanced Research in Applied Mechanics* 99, no. 1 (2022): 10-23.